



Preparation and Thermophysical Investigations of CoFe₂O₄-based Nanofluid: a Potential Heat Transfer Agent

Prashant B. Kharat¹ · Jitendra S. Kounsalye¹ · Mahendra V. Shisode¹ · K. M. Jadhav¹

Received: 12 April 2018 / Accepted: 25 April 2018 / Published online: 11 May 2018
© Springer Science+Business Media, LLC, part of Springer Nature 2018

Abstract

Cobalt ferrite nanoparticles were synthesized by employing chemical co-precipitation technique. The structure, morphology, elemental composition, and magnetization studies of cobalt ferrite nanoparticles were carried by XRD, FE-SEM, EDS, and VSM techniques, respectively. Rietveld refined XRD pattern exhibited the single-phase cubic spinel structure with Fd-3m space group. FE-SEM images indicated some agglomeration of spherical grains which can be attributed to high surface energy and magnetic interactions. Presence of peaks of respective elements (Co, Fe, and O) in EDS spectrum showed formation of CoFe₂O₄. The M–H loop recorded at 300 K revealed superparamagnetic behavior and explained by fine particles size. The blocking temperature of the CoFe₂O₄ nanoparticles from FC-ZFC curve was found to be 144 K. Cobalt ferrite–ethylene glycol nanofluids of various concentrations 0.0–1.0% in steps of 0.2% were prepared by ultrasonically assisted two-step technique. Thermophysical parameters such as thermal conductivity, specific heat, viscosity, and density were investigated as a function of both volume fraction and temperature. The experimental and theoretical value of each sample was correlated. The thermal conductivity was significantly enhanced with an increase in volume fraction and temperature.

Keywords CoFe₂O₄ nanoparticles · Nanofluids · Ethylene glycol · Volume fraction · Temperature

Nomenclature

φ	Volume fraction (%)
λ	Wavelength of x-ray (Å)
χ^2	Goodness of fit
a	Lattice constant (Å)
ρ	Density (kg/m ³)
S	Specific surface area (m ² /g)
T_B	Blocking temperature (K)
M_S	Saturation magnetization (emu/gm)
M_R	Remanence magnetization (emu/gm)
H_C	Coercivity (Oe)
η_B	Magneton number
k	Thermal conductivity (W/mK)
C	Specific heat (J/(kg K))
μ	Viscosity (cP)

Subscripts

R_p, R_{wp}	Profile Reliability Index, Weighted Profile Reliability Index
nf	Nanofluids
p	Nanoparticles
f	Fluid

1 Introduction

Nanofluid consists of solid nanoparticles suspended in a carrier liquid such as water, oil, polyethylene glycol, and ethylene glycol. Nanofluids were initiated to have several attractive applications [1–11, 13–15], few of them are heating, ventilation, air conditioning and cooling [6], solar cells [7], sensor [4], etc. Typically, water, oil, and ethylene glycol possess low heat transfer capacities than the nanoparticles of Ag, Cu, CuO, Fe₂O₃, SiO₂, CoFe₂O₄, NiFe₂O₄, etc. with notable thermal conductivity. Spinel ferrite nanoparticles proved its potential use in nanofluid due to its robust nature [8]. Among carrier liquids, the low freezing point, high boiling point, and moderate heat transfer properties of ethylene glycol motivates its use as the carrier fluid in nanofluids [9]. Thus, the heat transfer

✉ Prashant B. Kharat
pbk9403750321@gmail.com
K. M. Jadhav
drjadhavkm@gmail.com

¹ Department of Physics, Dr. Babasaheb Ambedkar Marathwada University, Aurangabad, Maharashtra 431001, India

capacities of nanofluids significantly depend on thermal conductivity of nanoparticles suspended in base fluid. Besides excellent magnetic properties, thermal and heat transfer properties of cobalt ferrite (CoFe_2O_4) nanoparticles make it a potential material to augment the thermophysical properties of the nanofluid [10].

The heat transfer and its augmentation studies on CoFe_2O_4 and ethylene glycol-based nanofluids are described using useful medium theory (EMT) which is based on Maxwell's mean field theory. The reports on thermal conductivity augmentations are within [11] or beyond [12] the estimates of useful medium theory. Pastoriza-Gallego et al. [13], presented the thermal conductivity augmentation of Al_2O_3 -ethylene glycol nanofluid with both increases of particle concentration as well as temperature and the obtained values are over predicated values. Whereas his other work [14] reported that the thermal conductivity values are within estimated values for ethylene glycol-based Fe_2O_3 and Fe_3O_4 nanofluids. Zhu et al. [15] revealed that the available models in published studies underestimated the measured thermal conductivities of Fe_3O_4 aqueous nanofluid and observed that Fe_3O_4 nanofluids provided more excellent thermal conductivity compared to other nanofluids. Abareshi et al. [16] showed 11.5% rise in thermal conductivity by addition of 3 volume percent of Fe_3O_4 nanoparticles at 40 °C. Sundar et al. [17, 18] interpreted that the Brownian motion of nanoparticles was the main effective parameter to lead the augmentation of thermal conductivity. They developed a new correlation for thermal conductivity prediction regarding concentration along with the temperature. The effect of nanofluid concentration on thermal conductivity of Fe_3O_4 /water nanofluid was evaluated by Bahiraei and Hangi [19] and a nonlinear relationship was observed. They suggested the implementation of the neural network to predict the experimental results based on temperature and concentration. Moreover, Bahiraei [20] examined the migration of particles in Fe_3O_4 /water nanofluid and revealed that non-uniform distribution of thermal conductivity could be observed under non-uniformity of nanofluid concentration. From literature survey, it is clear that the thermal conductivity of nanofluids highly depends on the size, shape, and clustering of nanoparticles. Despite numerous studies [21, 22], the exact mechanism responsible for thermal conductivity augmentation remained uncertain because of the lack of molecular-level understanding of the ultrafine particle which demands the systematic studies on the molecular interactions of nanofluids at various concentrations and temperatures.

In the present work, the stable and homogeneous suspensions of CoFe_2O_4 nanoparticles in ethylene glycol with different volume fractions were prepared. A deep understanding of interactions of ferrite nanoparticles–fluid as a

function of concentration and temperature is the primary concern of the present work. The synthesis, characterization of cobalt ferrite nanoparticles, and investigation of thermophysical properties as well as validation with theoretical models of CoFe_2O_4 –ethylene glycol nanofluids are focused here. Moreover, it is intended to formulate a relationship between thermophysical properties and concentration of CoFe_2O_4 nanoparticles in nanofluids.

2 Materials and Methods

2.1 Materials

The raw materials to synthesize the cobalt ferrite nanoparticles as cobalt nitrate ($\text{Co}(\text{NO}_3)_2 \cdot 6\text{H}_2\text{O}$), ferric nitrate ($\text{Fe}(\text{NO}_3)_3 \cdot 9\text{H}_2\text{O}$), sodium hydroxide (NaOH), and distilled water (H_2O) were used. Moreover, acetone ($(\text{CH}_3)_2\text{CO}$) and nitric acid (HNO_3) is used for impurity removal of the precipitate, if any. Furthermore, ethylene glycol ($\text{C}_2\text{H}_6\text{O}_2$) was employed to prepare nanofluid. All raw materials were procured by Merck of analytical reagent (AR) grade and used as supplied without any further purification.

2.2 Synthesis

Cobalt ferrite nanoparticles were synthesized using coprecipitation wet chemical technique [23, 24]. The weighed amount of nitrates of respective sources was dissolved in distilled water separately in the stoichiometric ratio as 1:2 (cobalt nitrate/ferric nitrate). The solutions of both nitrates were mixed and stirred to get a homogeneous mixture [8]. The pH of the mixed solution was adjusted at 9 by adding 2-M sodium hydroxide solution drop by drop. The obtained black precipitate was heated at 90 °C for 2 h and was allowed to cool. Then, it was washed several times with distilled water to remove impurities. An aqueous solution of 2-M nitric acid was added to the precipitate and stirred for 1 h. The supernatant solution was removed, and the residue was cleaned using distilled water and acetone [23]. CoFe_2O_4 nanoparticles were dispersed in ethylene glycol by employing ultrasonication for 3 h to get a homogenous suspension without any phase separation and sedimentation. The nanofluids of varying volume fraction as 0.0, 0.2, 0.4, 0.6, 0.8, and 1.0% were prepared. A detailed flowchart of synthesis and preparation of cobalt ferrite–ethylene glycol nanofluid is shown in Fig. 1.

2.3 Characterizations

The structural analysis of CoFe_2O_4 nanoparticles was carried out by x-ray diffraction (XRD) technique. XRD pattern of CoFe_2O_4 nanoparticles were obtained using

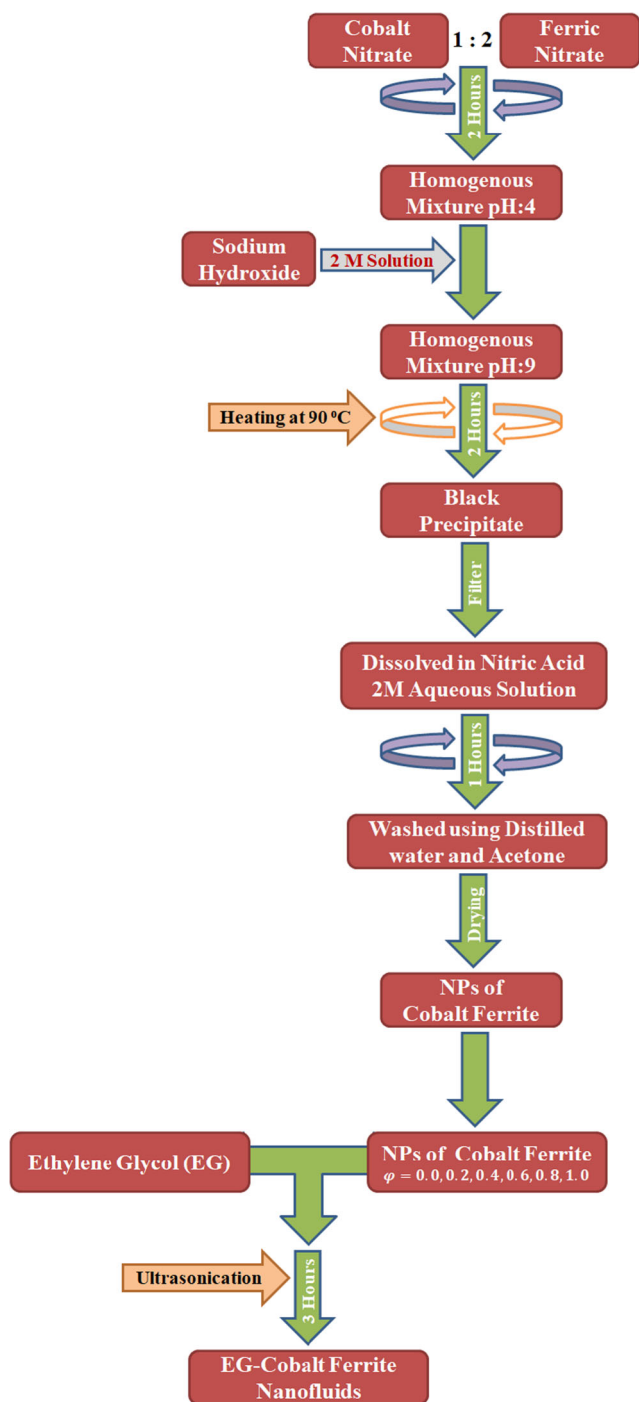


Fig. 1 Flowchart of synthesis and preparation of cobalt ferrite-ethylene glycol nanofluid

x-ray diffractometer in the 2θ range of $20\text{--}80^\circ$ with $\text{Cu-K}\alpha$ radiation ($\lambda = 1.506 \text{ \AA}$). The Rietveld refinement of XRD pattern was performed using FullProf program. The surface morphology and elemental composition of CoFe_2O_4 nanoparticles were examined by field emission scanning electron microscope (FE-SEM) equipped with energy-dispersive spectroscopy (EDS) unit, respectively.

Magnetic investigations of CoFe_2O_4 nanoparticles were carried out using vibrating sample magnetometer at room temperature with applied field $\pm 2 \text{ T}$. Field-cooled (FC) and zero-field-cooled (ZFC) curves were obtained by superconducting quantum interference device (SQUID) at a field of 100 Oe to study the low-temperature magnetization behavior. The thermophysical parameters such as thermal conductivity, specific heat capacity, density, and viscosity of CoFe_2O_4 -ethylene glycol nanofluid were measured by KD2 Pro - Decagon Devices, DSC-60 (Shimadzu Corporation), Anton-Paar portable density meter, and viscometer (Brookfield DV-III), respectively.

3 Results and Discussion

3.1 Structure, Morphology, and Magnetic Investigations

3.1.1 X-ray Diffraction and Rietveld Refinement

The x-ray diffraction and Rietveld refined XRD pattern of CoFe_2O_4 is presented in Fig. 2. In Fig. 2, the red line shows observed x-ray diffraction pattern, the black line represents calculated Rietveld refined pattern, and the blue line shows the difference between x-ray diffraction and Rietveld refined pattern of the cobalt ferrite nanoparticles. Green bars show the Bragg's position for the cobalt ferrite nanoparticles.

It shows the reflections as (200), (311), (222), (400), (422), (511), (440), (620), and (533) correspond to cubic spinel structure. It exhibits the Fd-3m space group [25, 26]. The experimental pattern match well with that of calculated as well as JCPDS number 96-591-0064. Rietveld refinement parameters as the goodness of fit (χ^2), profile reliability

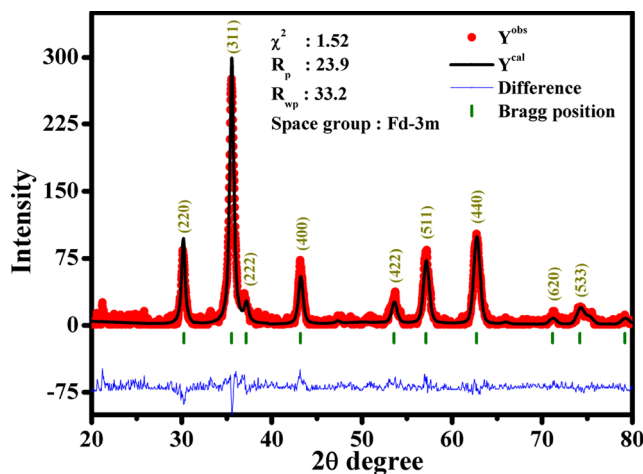


Fig. 2 X-ray diffraction and Rietveld refined pattern of cobalt ferrite nanoparticles

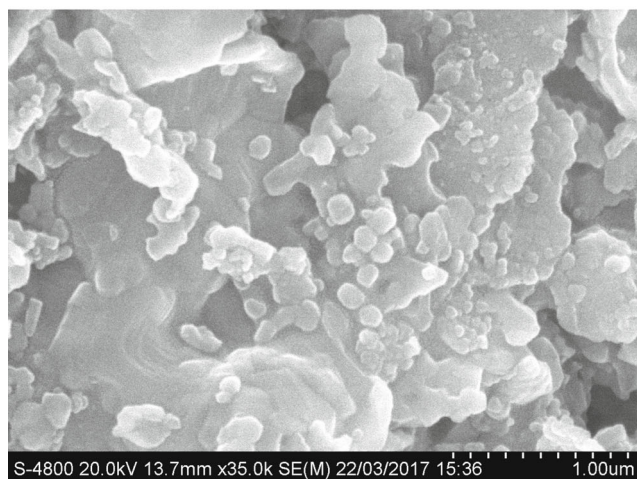
index (R_p), and weighted profile reliability index (R_{wp}) [27] are presented in Fig. 1. The broad peaks in XRD pattern indicate the fine particle nature and sufficiently small crystallite size. The highest intensity peak (311) was used to estimate the average crystallite size using Scherrer's formula [28] and found to be 11 nm. The lattice parameter a and x-ray density [29] ρ obtained from XRD data were found to be 8.374 Å and 537 kg/m³, respectively.

3.1.2 FE-SEM and EDS

The FE-SEM images of the CoFe₂O₄ sample are depicted in Fig. 3a, b. This figure shows the distribution of particle size is almost homogeneous and the average grain size are below 12 nm, confirming the nanocrystalline nature. Also, the agglomerations of nanoparticles were observed which may be attributed to the high surface energy and magnetic



(a) FE-SEM images of cobalt ferrite nanoparticles.



(b) FE-SEM images of cobalt ferrite nanoparticles.

Fig. 3 **a** FE-SEM images of cobalt ferrite nanoparticles. **b** FE-SEM images of cobalt ferrite nanoparticles

interactions of CoFe₂O₄ nanoparticles [30]. Morphology, particle size, and surface structure of nanoparticles may crucially depend on reaction conditions such as temperature, pH, and calcination temperature. It is reported that the pH of the precursors influences the morphologies of the nanoparticles in co-precipitation method [31]. The pH of the solvent is decreased with an increase in the concentration of dopants. Subsequently, high amounts of the agent (NaOH) are required to reach the suitable pH of the precipitation [30]. Therefore, the nucleation rate of precipitation and the morphology of nanoparticles may vary from one sample to another. Similar observations were reported [32] for nanocrystalline mixed spinel ferrite prepared using the wet chemical route. The specific surface S area was found 98 m²/g.

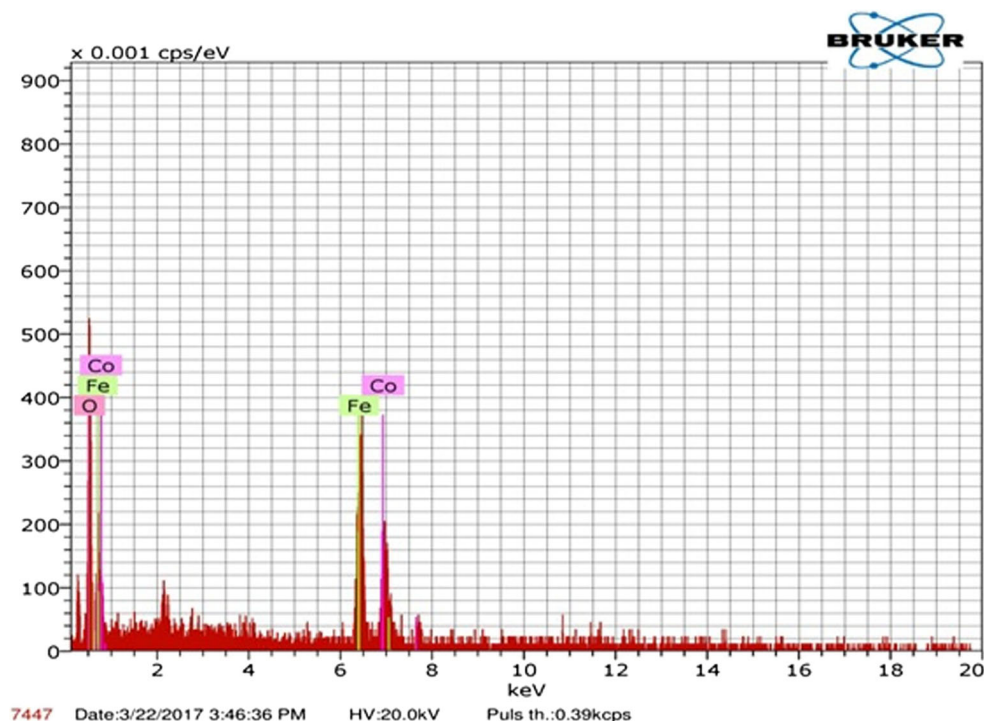
Figure 4 shows EDS spectrum of CoFe₂O₄ nanoparticles. The elemental composition of CoFe₂O₄ sample was quantitatively obtained from EDS spectrum. An EDS spectrum indicates the presence of peaks for Co, Fe, and O with no further impurity peak. The obtained atomic ratio of Co, Fe, and O match well with that of expected and maintains the stoichiometric proportion. It is worth mentioning here that the co-precipitation technique and the subsequent heat treatment highly favored the formation of the nanocrystalline CoFe₂O₄ sample.

3.1.3 Magnetization

Magnetization versus applied magnetic field (M – H) hysteresis loop of CoFe₂O₄ nanoparticles was recorded at 300 K using VSM and presented in Fig. 5. M – H plot shows that the magnetic anisotropy and magnetic moment per atom of cobalt ferrite nanoparticles is enhanced than those of their bulk form [33]. It is well recognized that a ferromagnetic material in bulk form is composed of very tiny regions, known as magnetic domains. These magnetic domains emerged from a balance of several terms viz. exchange energy, magnetocrystalline anisotropy, and magnetostatic energy [34].

The exchange energy makes an attempts to bring into line all magnetic moments in the similar direction, the magnetocrystalline anisotropy strives to orient magnetic moments along precise directions, and the magnetostatic energy seeks to abolish the magnetization in the material. In every domain, the magnetic moments of atoms are united in the single direction giving a net magnetization of all domains [35]. Hence, the net magnetization of a magnetic material originated from the addition of the different magnetizations of all magnetic domains [36]. It was found that the magnetic domains in ferromagnetic materials having very small size (less than 100 nm) below which the ferromagnetic material cannot split up further into domains and are called single or mono-domain particles [37].

Fig. 4 EDS spectrum of cobalt ferrite nanoparticles



Thermal energy plays an important role in the magnetic volatility of mono-domain magnetic particles. The CoFe_2O_4 might be composed of a mono-domain, under the critical limit of its size. It might also show a superparamagnetic nature above a specific temperature which is called as the blocking temperature (T_B) [38]. In the superparamagnetic form, the magnetic moments of the nanoparticles vary around the axes of magnetization. Thus, each one of the CoFe_2O_4 possesses a large magnetic moment that continuously changes its orientation [39]. When an external magnetic field is applied, CoFe_2O_4 in the

superparamagnetic form shows a quick response to the changing magnetic field along with less remanent magnetization and smaller coercivity. Thus, in the superparamagnetic form, CoFe_2O_4 nanoparticles act as a paramagnetic atom with a giant spin [40, 41].

The magnetic parameters like saturation magnetization (M_s), remanence magnetization (M_R), and coercivity (H_c) were obtained from M – H plot as 78.30 and 25.75 emu/gm and 149.86 Oe, respectively. On comparing obtained values of magnetic parameters with CoFe_2O_4 nanoparticles prepared using sol-gel auto combustion technique [42], it is found that the presently investigated material is superior. As cobalt ferrite nanoparticles prepared by sol-gel auto combustion technique exhibit 60.50 and 36 emu/gm and 1305-Oe saturation magnetization, remanence magnetization, and coercivity, respectively. It can be explained by the smaller particle size of the present sample. As particle size decreases, the saturation and remanence magnetization enhances and coercivity decreases. The magnetic behavior of present CoFe_2O_4 nanoparticles can be explained by Neel’s ferrimagnetism model [43]. Using Neel’s model the theoretical magneton number of CoFe_2O_4 nanoparticles was calculated as

$$\eta_B = M_B - M_A \tag{1}$$

where M_B and M_A are the magnetic moments of octahedral and tetrahedral sites, respectively. It is a well-known fact that the Co^{2+} has a preference to octahedral B sites and Fe^{3+} occupies each tetrahedral site as well as the octahedral site [29]. However, Co^{2+} ions have octahedral

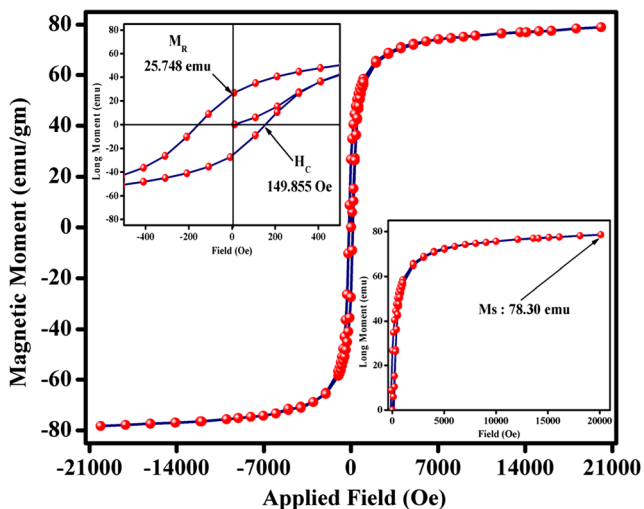


Fig. 5 M – H plot of cobalt ferrite nanoparticles recorded at 300 K

site preference it must occupy tetrahedral A sites. As cobalt ions have magnetic moment $3 \mu_B$ and Fe^{3+} ions as $5 \mu_B$. Co^{2+} ions occupy A site by replacing Fe^{3+} ions thereby decreasing the magnetic moment of A sites. Thus, net magnetic moment increases with Co^{2+} ions. The experimental magneton number obtained was $3.28 \mu_B$ and that of calculated using Neel's model was $3.4 \mu_B$. This indicates that Co^{2+} ions partially occupied tetrahedral A sites. The resulting cation distribution can be written as $(Co_{0.1}Fe_{0.9})^A (Co_{0.9}Fe_{1.1})^B$. Similar cation distribution as $(Co_{0.095}Fe_{0.905})^A (Co_{0.905}Fe_{1.095})^B$ was deduced from XRD pattern of the presently investigated sample. Thus, it is well-supported and confirmed the Co^{2+} ions distribution over both sub-lattices.

3.1.4 Low-Temperature Magnetization

Thermal behavior of nanoparticles is studied for the confirmation of superparamagnetism and to study the effect of temperature on magnetic properties. The commonly used technique for the investigation of superparamagnetic relaxation is the field-cooled (FC) and zero-field-cooled (ZFC) magnetization, that is, the magnetization in a weak applied field as a function of increasing temperature after the sample has been cooled, respectively, in the presence and absence of a weak magnetic field [44, 45]. Figure 6 shows the temperature-dependent ZFC and FC curves for the sample. Generally, from the graph, it can be seen from the ZFC measurements the $CoFe_2O_4$ was cooled from room to a low temperature in the absence of magnetic field. Then, a small magnetic field (about 100 Oe) is applied and the magnetization is measured as the temperature was being raised. As temperature increases, thermal energy will cause the moments to align along the direction of

the applied magnetic field. The number of these aligned moments will increase as the temperature increases reaching a maximum at T_B [46]. As the temperature is raised above T_B , the thermal energy becomes large enough to cause the magnetic moments to flip randomly which results in a suppression of the magnetization of the particle. The ZFC curve reached a maximum at 144 K for $CoFe_2O_4$ and this is considered as the blocking temperature of the sample (T_B). At temperatures below the blocking temperature, the thermal agitation becomes small and will not be able to cause fluctuations in the orientations of the magnetic moments of the nanoparticles where they freeze in random orientations. Hence, the $CoFe_2O_4$ sample shows superparamagnetic nature [47, 48]. However, the superimposition of FC-ZFC takes place at 166 K for $CoFe_2O_4$ sample. The superimposition of FC-ZFC curves is the typical characteristic feature of the superparamagnetic system [49, 50]. The superparamagnetism is induced in the system when the system's transfer from multi-domain to single and uniformly magnetized domains. The overall system is then in a state of uniform magnetization and its phase transition occurs from and ferromagnetic to superparamagnetic [51].

In FC measurements, the $CoFe_2O_4$ was cooled from room temperature to a low temperature in the existence of magnetic field. The magnetization is measured as the temperature was being cooled. At $T > T_B$, thermal energy was large enough to randomize the magnetic moments in the particle leading to very small net magnetization [52]. As the temperature is lowered, thermal energy decreased and for some moments, it becomes smaller than that produced by the aligning field. This causes some moments to align along the field direction leading to an increase in magnetization [53]. As the temperature decreases further, more and more moments will be frozen along the direction of the applied field. The magnetization of the $CoFe_2O_4$ expected to keep increasing down to the lowest temperature in single-domain nanoparticles [54].

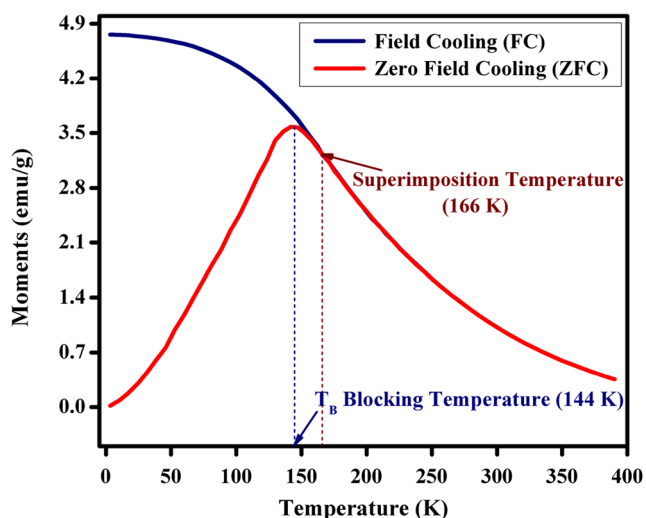


Fig. 6 Zero-field cooling (ZFC) and field-cooling (FC) curve of the cobalt ferrite nanoparticles

3.2 Thermophysical Investigations

3.2.1 Thermal Conductivity

In the present study, the thermal conductivity of the $CoFe_2O_4$ –ethylene glycol nanofluids was measured by using a KD2 Pro (Decagon Devices, Inc., USA) thermal properties analyzer with a maximum error of about 5%. This device employs the transient hot wire (THW) technique to measure the thermal conductivity of nanofluid which is a fast and reliable method [55, 56]. In order to measure the thermal conductivity of the samples, a cylindrical testing chamber with a diameter of 30 mm and length of 100 mm was used. After loading nanofluids into the

cylindrical testing chamber, the KD2 Pro KS-1 (stainless steel single needle) sensor, with length of 60 mm and diameter of 1.27 mm was vertically inserted into the center of nanofluids. This sensor has been especially proposed to measure the thermal conductivity of most fluids. The needle approximates the infinite line heat source. Each measurement cycle is the 60s. Heat is applied for the 30s. Thirty seconds are allowed for temperature equilibration before heating starts. After the reading, the controller computes thermal conductivity using the change in temperature. The thermal conductivity of fluids can be obtained by the following equation:

$$k = \frac{q(\ln t_2 - \ln t_1)}{4(\Delta T_2 - \Delta T_1)} \tag{2}$$

where q is the constant heat rate and ΔT_2 and ΔT_1 are the changes in temperature at times t_2 and t_1 , respectively. It should be noted that a stable temperature bath was used to stabilize the temperature of the samples. All the measurements of the thermal conductivity were repeated three times, which the average values of repeated measurements were recorded. The interval between two single measurements was 10 min.

Figure 7 shows the variation in thermal conductivity of cobalt ferrite ethylene glycol-based nanofluid as a function of nanoparticle volume fraction at various temperatures. The thermal conductivity significantly increases with increase in nanoparticles volume fraction. A similar trend was obtained experimentally at each temperature. It demonstrates that addition of nanoparticle volume fraction improves the thermal conductivity of nanofluid. It can be explained by the higher thermal conductivity of cobalt ferrite nanoparticles than carrier liquids. The thermal conductivity of presently investigated CoFe_2O_4 nanoparticles was 4.1 W/mK and that

of ethylene glycol is 0.25 W/mK. Hence, the addition of CoFe_2O_4 nanoparticles enhanced the thermal conductivity of nanofluid. Enhancement in thermal conductivity of nanofluid with cobalt ferrite nanoparticles can further explain by the Brownian motion [57], the creation of complexes and collisions between them, and clustering and layer formation of fluid molecules with nanoparticles surface [58]. The clustering leads to path creation with lower thermal resistance [59], which results in heat transfer enhancement in the fluid. The magnitude of clusters is a function of nanoparticle dimension and its volume fraction. Thus, this phenomenon can influence the thermal conductivity of nanofluids [60]. It is well accepted that the smaller clusters have an extensive effect on thermal conductivity of nanofluids. The higher volume fraction leads to the smaller distance between the nanoparticles; consequently, the probability of formation of cluster attraction increases. When the clustering takes place, the active surface area to volume ratio reduces; thereby resulting thermal conductivity reduction. Thus, more volume fraction leads to moderate enhancement in the thermal conductivity. It is precisely observed from Fig. 7 that the thermal conductivity enhancement above 0.4% volume fraction is lower than that up to 0.2% volume fraction. The higher nanoparticle volume fraction may increase the average dimension of the clusters. Hence, less degree of enhancement in thermal conductivity may occur. The thermal conductivity measurements show the maximum enhancement of $\sim 30\%$ in 1% volume fraction at 80 °C. The thermal conductivity of nanofluids can be estimated by either static or dynamic model. The existing theoretical models [57], the static model nanoparticles are assumed to be motionless in the base fluid; wherein thermal conductivity is predicted by the conduction-based model. Hence, the interfacial solid-liquid nanolayer results in unique thermophysical signature by differing to that of particles or fluid. The dynamic model works on the Brownian motion which is responsible for energy transport and turned as an efficient heat-transfer mechanism. The small clusters suspended in the fluid move faster and result in better energy transport. Hence, the Brownian motion contribution enhances the thermal conductivity.

$$\frac{k_{nf}}{k_f} = \frac{k_p + 2k_f + 2\phi(k_p + k_f)}{k_p + 2k_f + \phi(k_p + k_f)} \tag{3}$$

Moreover, Fig. 7 also depicts the variations of nanofluids thermal conductivity versus temperature for various nanofluid CoFe_2O_4 -ethylene glycol samples. Generally, it can be observed that with an increase in temperature, the thermal conductivity increases generally. The main reason of thermal conductivity enhancing due to the temperature increase can be characterized by Brownian motion, the loosening of the intermolecular bonds in the fluid layers, an

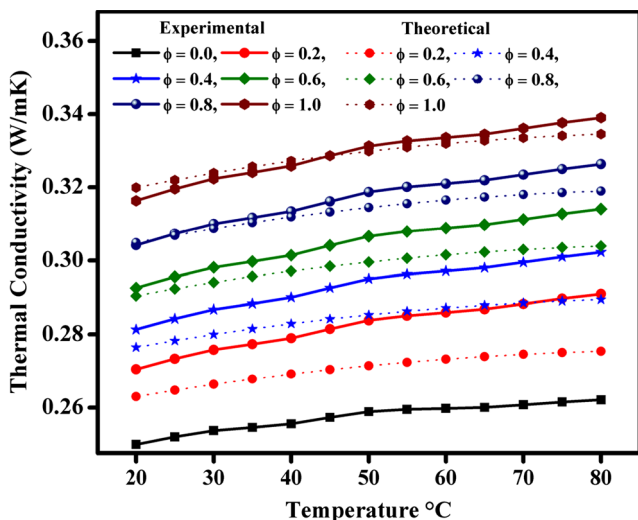


Fig. 7 Variation in thermal conductivity of cobalt ferrite–ethylene glycol nanofluids with temperature

increase in the number of collisions between nanoparticles; this causes the increase in interactions between the nanoparticles [56, 61]. Nanoparticle movement increases with rising temperature, and thermal conductivity improves due to a greater number of collisions between surface atoms with fluid molecules. However, the thermal conductivity of ethylene glycol considerably enhanced with increasing temperature, while the thermal conductivity of nanofluid slightly enhances. In fact, when nanoparticles are present in the ethylene glycol, the creation of nano-clusters takes place. Therefore, the Brownian motion is limited due to van der Waals forces; as a result, the effect of temperature becomes lower [60, 62]. Temperature and volume fraction significantly affects the thermal conductivity ratio of nanofluids. From the observations, it reveals that the thermal conductivity ratio of nanofluids enhanced with increasing temperature as well as volume fraction.

Furthermore, Fig. 7 indicates that the thermal conductivity curves of CoFe₂O₄-ethylene glycol nanofluid system slightly follow the theoretical curves for 0.2 and 0.4 volume fractions. However, remaining volume fraction curves closely follow theoretical curves with a minor difference.

3.2.2 Specific Heat Analysis

The specific heat (C_{nf}), a thermophysical quantity, of a nanofluid is estimated based on the physical principle of the mixture rule [63] as,

$$C_{nf} = \frac{\phi\rho_p C_p + (1 - \phi)\rho_f C_f}{\phi\rho_p + (1 - \phi)\rho_f} \tag{4}$$

where ρ_p is the density of nanoparticles, C_p is the specific heat of nanoparticles, ρ_f is density heat of base liquid, C_f is specific heat of base liquid, and ϕ is volume fraction.

The experimentally obtained specific heat for each sample has a considerable deviation with that of theoretical value (Fig. 8). It was found to decrease with increasing volume fraction, but as a function of temperature, it increases with a rise in temperature. The observed deviation is likely due to the formation of nanolayer between the nanoparticle and the fluid. A well-known fact is that the specific heat capacity depends on the bulk phases and the nature of interfacial nanolayers. As the surface of the nanoparticles has multiple phases, the specific heat decreases with volume fraction.

3.2.3 Viscosity Analysis

Figure 9 shows the viscosity of the nanofluid as a function of the temperature of varying volume fraction. It reveals the increase in viscosity with increasing volume fraction from 11 to 55 cP. The viscosity plays a vital role in momentum transfer between liquid layers and withstands

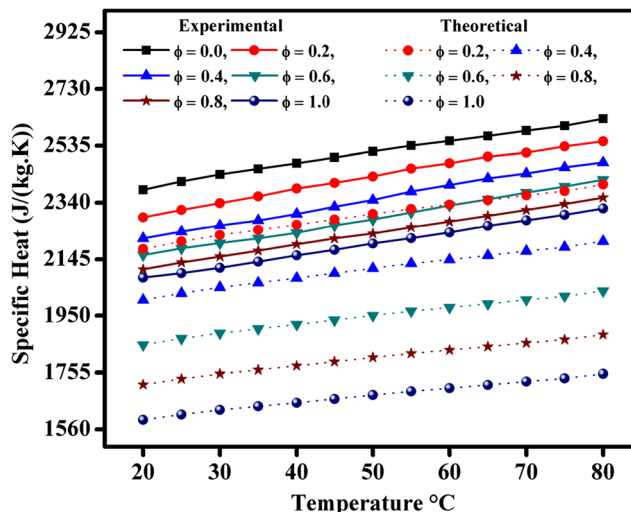


Fig. 8 Variation in specific heat of cobalt ferrite-ethylene glycol nanofluids with temperature

the relative movement of the liquid [64]. This phenomenon resulted by the Van der Waals forces between the molecules [65]. Therefore, the cobalt ferrite nanoparticles dispersion in ethylene glycol (EG) would increase the viscosity of the fluid. By increasing the number of nanoparticles in a specific amount of EG, larger nanoclusters arise due to the Van der Waals forces between them, which can prevent the movement of EG layers on each other. It may lead to improvement in viscosity of nanofluid.

Primarily, temperature and particle volume fraction influence the viscosity of nanofluid. The effective viscosity (μ_{nf}) of a suspension of solids may be written [4, 66] as:

$$\frac{\mu_{nf}}{\mu_f} = 1 + 2.5\phi \tag{5}$$

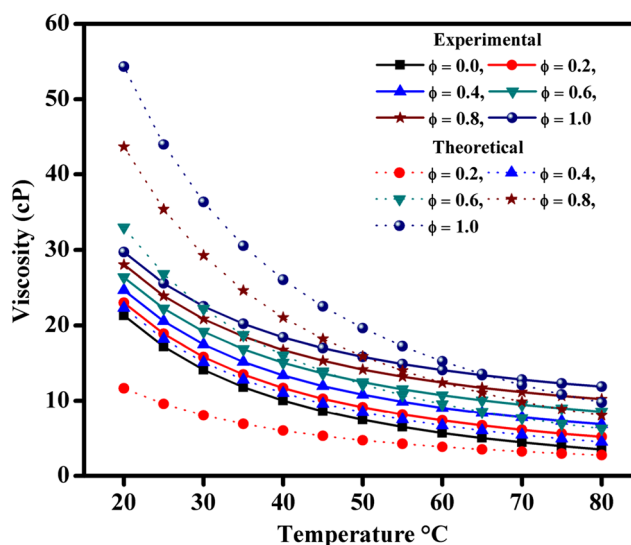


Fig. 9 Variation in viscosity of cobalt ferrite-ethylene glycol nanofluids with temperature

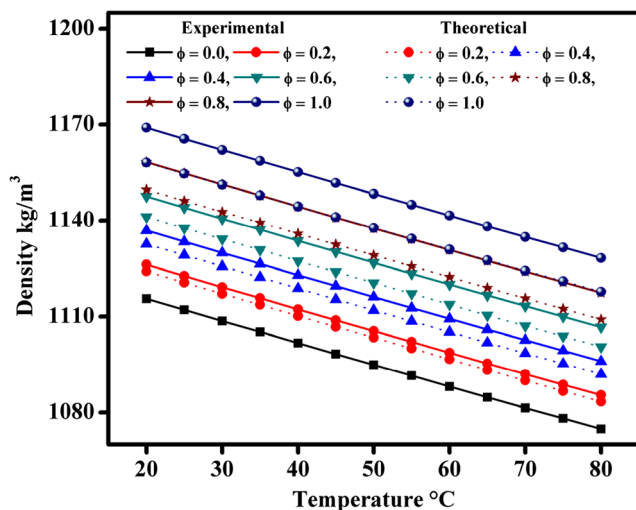


Fig. 10 Variation in the density of cobalt ferrite–ethylene glycol nanofluids with temperature

where φ is the volume fraction of the nanoparticles and μ_f is the viscosity of the base fluid. Both experimental and theoretical results over the temperature range 20–50 °C reduce rapidly and profoundly different from each other. Beyond 55 °C, both experimental and theoretical results show good agreement. This naturally implies that non-Newtonian corrections are essential for nanofluids such as this. Once again, the interfacial layer between the nanoparticles and fluid seem to be relevant.

It is noted from Fig. 9 that the viscosity of nanofluid reduces with the rise in temperature. As temperature increases, the intermolecular interactions between the molecules weaken and the viscosity reduces. Moreover, it is observed that the higher the volume fraction, the greater the effect of temperature viscosity. In addition to the interfacial effect pointed above, the probability of agglomeration of nanoparticles in the base fluid increases and viscosity significantly affected by volume fraction.

3.2.4 Density Analysis

Figure 10 shows the density of the nanofluid as a function of the temperature of varying volume fractions. The density is a significant physical property of the fluid and affects the friction factor, pump loss, and Reynolds number [67, 68]. It is directly related to particle volume fraction.

In the present investigation as shown in Fig. 8, it rises approximately in a linear manner with volume fraction and decreases with increase in temperature. The increasing nanoparticles volume fraction and these nanoparticles were increased crowd per unit volume. It causes agglomeration, hence, the density enhancement. The enhancement in the density of CoFe_2O_4 -ethylene glycol mainly owed to the fact of a denser nature of ethylene glycol. The

theoretical model accounts for the variation of concentration at various temperatures. To determine the rheology of suspensions, volume concentration is often used instead of mass concentration. Once the particle volume concentration is determined, the density of the nanofluid (ρ_{nf}) can be determined from,

$$\rho_{nf} = \varphi_p \rho_p + (1 - \varphi) \rho_f \quad (6)$$

where ρ_p is the density of particles, ρ_f is the density of the base liquid, and φ_p is the volume fraction of the particles. The decrease in density with temperature is due to the weakening of bonds at elevated temperature [69]. It can be noted that the obtained values of densities are within the range. Further, it is noted that the experimental curves follow the theoretical curves for 0.2–0.6 volume fractions. However, the theoretical curves of 0.8 and 1.0 volume fraction possess a smaller difference.

4 Conclusions

The single phase with Fd-3m space group CoFe_2O_4 nanoparticles were synthesized successfully using co-precipitation technique. The morphology revealed spherical nature and some of the agglomerations. M–H loop favored the superparamagnetic nature of CoFe_2O_4 nanoparticles. The low-temperature magnetization reveals the blocking temperature of the CoFe_2O_4 curve is of 144 K. The stable CoFe_2O_4 -ethylene glycol based nanofluid of varying volume fractions prepared using the ultrasonically assisted technique. The experimental results indicated significant augmentation in thermal conductivity with both nanoparticle volume fraction and temperature. The specific heat was decreased with nanoparticles volume fractions and augmented with the rise in temperature. The viscosity showed that each sample exhibit the Newtonian behavior. The proposed correlation between thermal conductivity and the experimental results revealed high accuracy.

Acknowledgments The authors are thankful to Professor John Philip, Indira Gandhi Center for Atomic Research Center, Kalpakkam, Tamilnadu, as well as Professor J. B. Naik, Head, University Institute of Chemical Technology, North Maharashtra University, Jalgaon, Maharashtra, for providing thermal conductivity and specific heat measurement facilities.

References

- Shima, P., Philip, J.: Tuning of thermal conductivity and rheology of nanofluids using an external stimulus. *J. Phys. Chem. C* **115**, 20097–20104 (2011)
- Rashin, M.N., Hemalatha, J.: A novel ultrasonic approach to determine thermal conductivity in CuO -ethylene glycol nanofluids. *J. Mol. Liq.* **197**, 257–262 (2014)

3. Ashraf, M.W., Tayyaba, S., Afzulpurkar, N.: Micro electromechanical systems (MEMS) based microfluidic devices for biomedical applications. *Int. J. Mol. Sci.* **12**, 3648–3704 (2011)
4. Saidur, R., Leong, K., Mohammad, H.: A review on applications and challenges of nanofluids. *Renew. Sustain. Energy Rev.* **15**, 1646–1668 (2011)
5. Philip, J., Jaykumar, T., Kalyanasundaram, P., Raj, B.: A tunable optical filter. *Meas. Sci. Technol.* **14**, 1289 (2003)
6. Das, S.K., Choi, S.U., Yu, W., Pradeep, T.: *Nanofluids: science and technology*. Wiley, Hoboken (2007)
7. Hayat, T., Waqas, M., Shehzad, S., Alsaedi, A.: A model of solar radiation and Joule heating in magnetohydrodynamic (MHD) convective flow of thixotropic nanofluid. *J. Mol. Liq.* **215**, 704–710 (2016)
8. Kale, G., Humbe, A.V., Kharat, P., Bhoyar, D., Jadhav, K.: Tartaric acid a novel fuel approach: synthesis and characterization of CoFe₂O₄ nano particles
9. Mahadik, M.M., Kharat, P.B.: Aliphatic organic compounds: a substitute of ferrite materials in isolator for high frequency application
10. Peyghambarzadeh, S., Hashemabadi, S., Hoseini, S., Jamnani, M.S.: Experimental study of heat transfer enhancement using water/ethylene glycol based nanofluids as a new coolant for car radiators. *Int. Commun. Heat Mass Transf.* **38**, 1283–1290 (2011)
11. Zhang, X., Gu, H., Fujii, M.: Effective thermal conductivity and thermal diffusivity of nanofluids containing spherical and cylindrical nanoparticles. *Exp. Therm. Fluid Sci.* **31**, 593–599 (2007)
12. Patel, H.E., Sundararajan, T., Das, S.K.: An experimental investigation into the thermal conductivity enhancement in oxide and metallic nanofluids. *J. Nanoparticle Res.* **12**, 1015–1031 (2010)
13. Pastoriza-Gallego, M.J., Lugo, L., Legido, J.L., Piñeiro, M.M.: Thermal conductivity and viscosity measurements of ethylene glycol-based Al₂O₃ nanofluids. *Nanoscale Res. Lett.* **6**, 221 (2011)
14. Pastoriza-Gallego, M.J., Lugo, L., Legido, J.L., Piñeiro, M.M.: Rheological non-Newtonian behaviour of ethylene glycol-based Fe₂O₃ nanofluids. *Nanoscale Res. Lett.* **6**, 560 (2011)
15. Zhu, H., Zhang, C., Liu, S., Tang, Y., Yin, Y.: Effects of nanoparticle clustering and alignment on thermal conductivities of Fe₃O₄ aqueous nanofluids. *Appl. Phys. Lett.* **89**, 023123 (2006)
16. Abareshi, M., Goharshadi, E.K., Zebarjad, S.M., Fadafan, H.K., Youssefi, A.: Fabrication, characterization and measurement of thermal conductivity of Fe₃O₄ nanofluids. *J. Magn. Mater.* **322**, 3895–3901 (2010)
17. Sundar, L.S., Singh, M.K., Sousa, A.C.: Investigation of thermal conductivity and viscosity of Fe₃O₄ nanofluid for heat transfer applications. *Int. Commun. Heat Mass Transf.* **44**, 7–14 (2013)
18. Sundar, L.S., Singh, M.K., Sousa, A.C.: Thermal conductivity of ethylene glycol and water mixture based Fe₃O₄ nanofluid. *Int. Commun. Heat Mass Transf.* **49**, 17–24 (2013)
19. Bahiraei, M., Hangi, M.: An empirical study to develop temperature-dependent models for thermal conductivity and viscosity of water-Fe₃O₄ magnetic nanofluid. *Mater. Chem. Phys.* **181**, 333–343 (2016)
20. Bahiraei, M.: Effect of particle migration on flow and heat transfer characteristics of magnetic nanoparticle suspensions. *J. Mol. Liq.* **209**, 531–538 (2015)
21. Sheikholeslami, M., Hatami, M., Ganji, D.: Nanofluid flow and heat transfer in a rotating system in the presence of a magnetic field. *J. Mol. Liq.* **190**, 112–120 (2014)
22. Mohebbi, A.: Prediction of specific heat and thermal conductivity of nanofluids by a combined equilibrium and non-equilibrium molecular dynamics simulation. *J. Mol. Liq.* **175**, 51–58 (2012)
23. Kharat, P.B., Shisode, M., Birajdar, S., Bhoyar, D., Jadhav, K.: Synthesis and characterization of water based NiFe₂O₄ ferrofluid. In: AIP Conference Proceedings, p. 050122. AIP Publishing (2017)
24. Kharat, P.B., Kounsalye, J.S., Humbe, A.V., Birajdar, S.D., Jadhav, K.: Preparation and diverse properties of cobalt ferrite ferrofluid
25. Kounsalye, J.S., Kharat, P.B., Chavan, A.R., Humbe, A.V., Borade, R., Jadhav, K.: Symmetry transition via tetravalent impurity and investigations on magnetic properties of Li_{0.5}Fe_{2.5}O₄. In: AIP Conference Proceedings, p. 050067. AIP Publishing (2018)
26. Kounsalye, J.S., Kharat, P.B., Bhoyar, D.N., Jadhav, K.: Radiation-induced modifications in structural, electrical and dielectric properties of Ti⁴⁺ ions substituted Li_{0.5}Fe_{2.5}O₄ nanoparticles. *J. Mater. Sci. Mater. Electron.* **29**(10):8601–8609
27. Kounsalye, J.S., Kharat, P.B., Shisode, M.V., Jadhav, K.: Influence of Ti⁴⁺ ion substitution on structural, electrical and dielectric properties of Li_{0.5}Fe_{2.5}O₄ nanoparticles. *J. Mater. Sci. Mater. Electron.* **28**, 17254–17261 (2017)
28. Chavan, A.R., Chilwar, R.R., Kharat, P.B., Jadhav, K.: Effect of annealing temperature on structural, morphological, optical and magnetic properties of NiFe₂O₄ thin films. *J. Supercond. Nov. Magn.* (2018). <https://doi.org/10.1007/s10948-018-4565-3>
29. Humbe, A.V., Kharat, P.B., Nawle, A.C., Jadhav, K.: Nanocrystalline Ni_{0.70-x}Cu_xZn_{0.30}Fe₂O₄ with 0 ≤ x ≤ 0.25 prepared by nitrate-citrate route: structure, morphology and electrical investigations. *J. Mater. Sci. Mater. Electron.* **29**, 3467–3481 (2018)
30. Alam, R.S., Moradi, M., Rostami, M., Nikmanesh, H., Moayed, R., Bai, Y.: Structural, magnetic and microwave absorption properties of doped Ba-hexaferrite nanoparticles synthesized by co-precipitation method. *J. Magn. Mater.* **381**, 1–9 (2015)
31. Shannugavani, A., Selvan, R.K., Layek, S., Vasylechko, L., Sanjeeviraja, C.: Influence of pH and fuels on the combustion synthesis, structural, morphological, electrical and magnetic properties of CoFe₂O₄ nanoparticles. *Mater. Res. Bull.* **71**, 122–132 (2015)
32. Humbe, A.V., Nawle, A.C., Shinde, A., Jadhav, K.: Impact of Jahn Teller ion on magnetic and semiconducting behaviour of Ni-Zn spinel ferrite synthesized by nitrate-citrate route. *J. Alloys Compd.* **691**, 343–354 (2017)
33. Obaidat, I.M., Issa, B., Haik, Y.: Magnetic properties of magnetic nanoparticles for efficient hyperthermia. *Nanomaterials* **5**, 63–89 (2015)
34. Tumanski, S.: *Handbook of magnetic measurements*. CRC Press, Boca Raton (2016)
35. Yadav, R.: Synthesis and characterization of structural and magnetic properties of electrodeposited cobalt iron thin film. In: Indian Institute of Technology Hyderabad (2015)
36. Yu, G., Upadhyaya, P., Fan, Y., Alzate, J.G., Jiang, W., Wong, K.L., Takei, S., Bender, S.A., Chang, L.-T., Jiang, Y.: Switching of perpendicular magnetization by spin-orbit torques in the absence of external magnetic fields. *Nat. Nanotechnol.* **9**, 548 (2014)
37. Srdić, V.V., Cvejić, Z., Milanović, M., Stojanović, G., Rakić, S.: Metal oxide structure, crystal chemistry, and magnetic properties. In: *Magnetic, Ferroelectric, and Multiferroic Metal Oxides*, pp. 313–332. Elsevier (2018)
38. Kolen'ko, Y.V., Baniñobre-Loópez, M., Rodríguez-abreu, C., Carboó-Argibay, E., Sailsman, A., Piñeiro-Redondo, Y., Cerqueira, M.F., Petrovykh, D.Y., Kovnir, K., Lebedev, O.I.: Large-scale synthesis of colloidal Fe₃O₄ nanoparticles exhibiting high heating efficiency in magnetic hyperthermia. *J. Phys. Chem. C* **118**, 8691–8701 (2014)

39. Gonçalves, E., Cornejo, D., Oliveira, C., Neto, A.F., Depeyrot, J., Tourinho, F., Aquino, R.: Magnetic and structural study of electric double-layered ferrofluid with $\text{MnFe}_2\text{O}_4/\gamma\text{-Fe}_2\text{O}_3$ nanoparticles of different mean diameters: determination of the magnetic correlation distance. *Phys. Rev. E* **91**, 042317 (2015)
40. Sharma, S.K.: Exchange bias: from thin film to nanogranular and bulk systems. CRC Press, Boca Raton (2017)
41. Zhang, S., Zhao, D.: Advances in magnetic materials: processing, properties, and performance. CRC Press, Boca Raton (2017)
42. Gharibshahian, M., Mirzaee, O., Nourbakhsh, M.: Evaluation of superparamagnetic and biocompatible properties of mesoporous silica coated cobalt ferrite nanoparticles synthesized via microwave modified Pechini method. *J. Magn. Magn. Mater.* **425**, 48–56 (2017)
43. Humbe, A.V., Kounsalye, J.S., Shisode, M.V., Jadhav, K.: Rietveld refinement, morphology and superparamagnetism of nanocrystalline $\text{Ni}_{0.70-x}\text{Cu}_x\text{Zn}_{0.30}\text{Fe}_2\text{O}_4$ spinel ferrite. *Ceramics International* (2017)
44. Khot, V., Salunkhe, A., Ruso, J., Pawar, S.: Improved magnetic induction heating of nanoferrites for hyperthermia applications: correlation with colloidal stability and magneto-structural properties. *J. Magn. Magn. Mater.* **384**, 335–343 (2015)
45. Kandasamy, G., Maity, D.: Recent advances in superparamagnetic iron oxide nanoparticles (SPIONs) for in vitro and in vivo cancer nanotheranostics. *Int. J. Pharm.* **496**, 191–218 (2015)
46. Khot, V., Salunkhe, A., Thorat, N., Ningthoujam, R., Pawar, S.: Induction heating studies of dextran coated MgFe_2O_4 nanoparticles for magnetic hyperthermia. *Dalton Trans.* **42**, 1249–1258 (2013)
47. Koksharov, Y.A.: Magnetism of nanoparticles: effects of size, shape, and interactions. *Magnetic nanoparticles:2011* (2009)
48. Salunkhe, A., Khot, V., Phadatar, M., Thorat, N., Joshi, R., Yadav, H., Pawar, S.: Low temperature combustion synthesis and magnetostructural properties of Co–Mn nanoferrites. *J. Magn. Magn. Mater.* **352**, 91–98 (2014)
49. Leufke, P.M.: Magnetolectric coupling in layered LSMO/PZT nanostructures, In: Technische universität (2014)
50. Nikam, D., Jadhav, S., Khot, V., Phadatar, M., Pawar, S.: Study of AC magnetic heating characteristics of $\text{Co}_0.5\text{Zn}_0.5\text{Fe}_2\text{O}_4$ nanoparticles for magnetic hyperthermia therapy. *J. Magn. Magn. Mater.* **349**, 208–213 (2014)
51. Rosensweig, R.E.: Ferrohydrodynamics, Courier Corporation (2013)
52. Bhuiya, A.W.: Temperature-induced phenomena in systems of magnetic nanoparticles. The University of Texas at El Paso (2009)
53. Issa, B., Obaidat, I.M., Albiss, B.A., Haik, Y.: Magnetic nanoparticles: surface effects and properties related to biomedicine applications. *Int. J. Mol. Sci.* **14**, 21266–21305 (2013)
54. Evans, M., Heller, F.: Environmental magnetism: principles and applications of enviromagnetics. Academic Press, Cambridge (2003)
55. Manimaran, R., Palaniradja, K., Alagumurthi, N., Sendhilnathan, S., Hussain, J.: Preparation and characterization of copper oxide nanofluid for heat transfer applications. *Appl. Nanosci.* **4**, 163–167 (2014)
56. Paul, G., Chopkar, M., Manna, I., Das, P.: Techniques for measuring the thermal conductivity of nanofluids: a review. *Renew. Sustain. Energy Rev.* **14**, 1913–1924 (2010)
57. Leong, K., Ahmad, K.K., Ong, H.C., Ghazali, M., Baharum, A.: Synthesis and thermal conductivity characteristic of hybrid nanofluids—a review. *Renew. Sustain. Energy Rev.* **75**, 868–878 (2017)
58. Yu, W., Xie, H.: A review on nanofluids: preparation, stability mechanisms, and applications. *J. Nanomater.* **2012**, 1 (2012)
59. Karthikeyan, N., Philip, J., Raj, B.: Effect of clustering on the thermal conductivity of nanofluids. *Mater. Chem. Phys.* **109**, 50–55 (2008)
60. Afrand, M.: Experimental study on thermal conductivity of ethylene glycol containing hybrid nano-additives and development of a new correlation. *Appl. Therm. Eng.* **110**, 1111–1119 (2017)
61. Toghraie, D., Chaharsoghi, V.A., Afrand, M.: Measurement of thermal conductivity of $\text{ZnO-TiO}_2/\text{EG}$ hybrid nanofluid. *J. Therm. Anal. Calorim.* **125**, 527–535 (2016)
62. Esfe, M.H., Karimipour, A., Yan, W.-M., Akbari, M., Safaei, M.R., Dahari, M.: Experimental study on thermal conductivity of ethylene glycol based nanofluids containing Al_2O_3 nanoparticles. *Int. J. Heat Mass Transf.* **88**, 728–734 (2015)
63. Gupta, A.K., Mishra, G., Nirmalkar, N., Chhabra, R.: Effect of confinement on heat transfer in aqueous nanofluids from a heated sphere. *Powder Technol.* **325**, 576–596 (2018)
64. Dardan, E., Afrand, M., Isfahani, A.M.: Effect of suspending hybrid nano-additives on rheological behavior of engine oil and pumping power. *Appl. Therm. Eng.* **109**, 524–534 (2016)
65. Kharat, P.B., Somvanshi, S.B., Kounsalye, J.S., Deshmukh, S.S., Khirade, P.P., Jadhav, K.: Temperature dependent viscosity of cobalt ferrite/ethylene glycol ferrofluids. In: AIP Conference Proceedings, p. 050044. AIP Publishing (2018)
66. Wu, J., Zhao, J.: A review of nanofluid heat transfer and critical heat flux enhancement—research gap to engineering application. *Prog. Nucl. Energy* **66**, 13–24 (2013)
67. Kandlikar, S., Garimella, S., Li, D., Colin, S., King, M.R.: Heat transfer and fluid flow in minichannels and microchannels. Elsevier, NY (2005)
68. Faghri, A.: Heat pipe science and technology. Global Digital Press, Kanpur (1995)
69. Suganthi, K.S., Anusha, N., Rajan, K.S.: Low viscous ZnO -propylene glycol nanofluid: a potential coolant candidate. *J. Nanoparticle Res.* **15**, 1986 (2013)